

# Catalysis Science & Technology

Accepted Manuscript



This is an *Accepted Manuscript*, which has been through the Royal Society of Chemistry peer review process and has been accepted for publication.

*Accepted Manuscripts* are published online shortly after acceptance, before technical editing, formatting and proof reading. Using this free service, authors can make their results available to the community, in citable form, before we publish the edited article. We will replace this *Accepted Manuscript* with the edited and formatted *Advance Article* as soon as it is available.

You can find more information about *Accepted Manuscripts* in the [Information for Authors](#).

Please note that technical editing may introduce minor changes to the text and/or graphics, which may alter content. The journal's standard [Terms & Conditions](#) and the [Ethical guidelines](#) still apply. In no event shall the Royal Society of Chemistry be held responsible for any errors or omissions in this *Accepted Manuscript* or any consequences arising from the use of any information it contains.

Cite this: DOI: 10.1039/c0xx00000x

www.rsc.org/xxxxxx

ARTICLE TYPE

# Facile Structure Design Based on C<sub>3</sub>N<sub>4</sub> for Mediator-free Z-Scheme Water Splitting under Visible Light

Guixia Zhao,<sup>‡</sup> Xiubing Huang,<sup>‡</sup> Federica Fina, Guan Zhang and John T.S. Irvine\*

Received (in XXX, XXX) Xth XXXXXXXXX 20XX, Accepted Xth XXXXXXXXX 20XX

DOI: 10.1039/b000000x

In this work, two photocatalysts (i.e., C<sub>3</sub>N<sub>4</sub> and WO<sub>3</sub>) were successfully combined into a heterojunction structure by a facile hydrothermal method for mediator-free overall water splitting, analogous to the natural photosynthesis over two-photo excited Z-scheme system. Hydrogen and oxygen are evolved with a 2:1 ratio by irradiating the C<sub>3</sub>N<sub>4</sub>-WO<sub>3</sub> composites loaded with Pt under visible light ( $\lambda > 420$  nm) without any redox mediator. Introducing reduced graphene oxide (rGO) to the C<sub>3</sub>N<sub>4</sub>-WO<sub>3</sub> composites enhances the water splitting efficiency. Through optimizing the mass ratio in the C<sub>3</sub>N<sub>4</sub>-WO<sub>3</sub> composites, rGO content, amount of loaded Pt and pH value of the reacting system, the highest H<sub>2</sub>/O<sub>2</sub> evolution rates of 2.84 and 1.46  $\mu\text{mol h}^{-1}$  can be obtained, with quantum yield of 0.9%. Our findings demonstrate that hydrothermal method is a promising strategy for constructing intimate heterostructures for Z-scheme water-splitting system without using any redox mediator, and that rGO can be used to further enhance the performance in optimized conditions.

## 1. Introduction

With the increasing energy demand and concerns about environmental issues, hydrogen gas is considered as a promising fuel because of its no carbon emission nor other harmful by-products.<sup>1</sup> The artificial photosynthesis for hydrogen generation through water splitting under visible light is an important approach, among which, the powdered-type two-step photoexcitation system, i.e., Z-scheme photocatalysis system, is the most similar to natural photosynthesis.<sup>2-6</sup> Normally, a Z-scheme system contains two photocatalysts (one for H<sub>2</sub> evolution, and the other for O<sub>2</sub> evolution) and usually an electron mediator, which transfers the electrons from the excited O<sub>2</sub> photocatalyst to the holes generated in the H<sub>2</sub> photocatalyst.<sup>7</sup>

It is suggested that electron transfer is the rate-determining process.<sup>8</sup> The commonly used electron mediators are ionic redox couples such as IO<sub>3</sub><sup>-</sup>/I<sup>-</sup>,<sup>2, 3, 9</sup> or Fe<sup>3+</sup>/Fe<sup>2+</sup>.<sup>4, 9, 10</sup> Compared with these ionic redox couples, solid electron shuttle is more advanced for the recycle of the photocatalyst and cleaning of water. The challenges for the efficient H<sub>2</sub>/O<sub>2</sub> evolution lie in the electron-accepting and -donating abilities of the mediator, which should retain a dynamic equilibrium and keep stable during reactions.<sup>11</sup> Furthermore, interface contact in the ternary system also plays an important role in maintaining continuous electron flow between the two photocatalysts. Considering the extremely high conductivity and specific surface area of graphene, it may be a good candidate as electron mediator for Z-scheme system.<sup>11</sup> Besides, it is also challenging to choose appropriate photocatalysts for realizing the intimate physical interaction with graphene, the efficient charge carrier separation, the H<sub>2</sub>/O<sub>2</sub> evolution on the H<sub>2</sub>/O<sub>2</sub> photocatalysts and then finally preventing water formation due to the backward reaction of H<sub>2</sub> and O<sub>2</sub>.<sup>12, 13</sup>

In Iwase et al's report,<sup>11</sup> it has been shown that photoreduced graphene oxide (PRGO) was able to function as a solid electron mediator for Z-scheme overall water splitting, where SrTiO<sub>3</sub>:Rh was used as H<sub>2</sub> evolution photocatalyst, with 0.7 wt% Ru as co-catalyst, and BiVO<sub>4</sub> was used as O<sub>2</sub> evolution photocatalyst. The PRGO was synthesized by photoreduction, i.e., irradiating the mixture of graphene oxide and the photocatalyst (Ru/SrTiO<sub>3</sub>:Rh or BiVO<sub>4</sub>) in the presence of methanol as electron donor. For the combined PRGO/BiVO<sub>4</sub> and Ru/SrTiO<sub>3</sub>:Rh under pH 3.5, the H<sub>2</sub> evolution rate is ca. 8  $\mu\text{mol h}^{-1}$ , while under the neutral condition, the performance is much lower, which is considered due to the bad physical interaction between the PRGO/BiVO<sub>4</sub> and Ru/SrTiO<sub>3</sub>:Rh under neutral conditions. In total, the reported Z-scheme based on PRGO is complicated in preparation as the noble metals (i.e., Ru and Rh) are used as co-catalyst and dopant, respectively, and the performance is dependent on the acidity. Although Sasaki et al.<sup>8</sup> reported the interparticle electron transfer without any electron mediator, the water splitting can only proceed efficiently by acidifying the aqueous solution to realize the effective contact through the aggregation of the two photocatalysts, Ru/SrTiO<sub>3</sub>:Rh and BiVO<sub>4</sub>. Thus, more sturdy contacts between the H<sub>2</sub>/O<sub>2</sub> evolution photocatalysts need to be found.

Since the introduction of graphitic carbon nitride (C<sub>3</sub>N<sub>4</sub>) into heterogeneous catalysis in 2006,<sup>14, 15</sup> this yellow polymer consisting of tri-s-triazines interconnected via tertiary amines has attracted increasing interest in material research especially in H<sub>2</sub>-evolution photocatalysis under visible light.<sup>16-18</sup> The band gap of C<sub>3</sub>N<sub>4</sub> is ca. 2.7 eV, with the CB and VB positions located at ca. -1.1 eV and ca. +1.6 eV vs normal hydrogen electrode (NHE), respectively.<sup>16, 19</sup> More importantly, the preparation of C<sub>3</sub>N<sub>4</sub> is

low cost since it only consists two elements (C and N). For O<sub>2</sub>-evolution photocatalysis from water, tungsten trioxide (WO<sub>3</sub>) has been widely investigated because of its suitable bandgap, high electron mobility, abundance and low cost.<sup>20</sup>

5 Herein, we introduced a novel method to generate a close contact between C<sub>3</sub>N<sub>4</sub> and WO<sub>3</sub> by the reaction of Na<sub>2</sub>WO<sub>4</sub>·2H<sub>2</sub>O and C<sub>3</sub>N<sub>4</sub> under hydrothermal conditions. To enhance the performance, rGO was also used to function as electron mediator. By calcining the mixture of rGO and melamine, the graphene  
10 layer was able to be homogeneously mixed with C<sub>3</sub>N<sub>4</sub> layers. Then through hydrothermal method, the C<sub>3</sub>N<sub>4</sub>-rGO composites were loaded with WO<sub>3</sub> particles, which function as O<sub>2</sub> evolution photocatalyst. It is demonstrated that the binary (in the case of no rGO) or ternary (in the case of containing rGO) composites were  
15 able to give out H<sub>2</sub> and O<sub>2</sub> under visible light irradiation ( $\lambda > 420$  nm) with relatively high performance when loaded with Pt as co-catalyst, and appropriate amount of rGO will enhance the performance.

## 2. Experimental Section

20 *Synthesis of C<sub>3</sub>N<sub>4</sub>-rGO composite and pure C<sub>3</sub>N<sub>4</sub>*: Graphene oxide was synthesized according to the modified Hummers method as described in our previous work.<sup>21</sup> The as-prepared GO was then reduced by hydrothermal method. 60 mg of GO was dissolved in 30 mL of H<sub>2</sub>O by moderate sonication and the pH was adjusted to  
25 about 7 using NaOH solution before transferred into a Teflon-lined steel autoclave, which was heated in an oven at 140 °C for 18 h. The obtained rGO was collected and washed with distilled water and ethanol several times, and dried at 90 °C for 2 h. C<sub>3</sub>N<sub>4</sub>-rGO composites were obtained by calcining the mixtures of  
30 melamine and rGO with different mass ratios. These C<sub>3</sub>N<sub>4</sub>-rGO composites are noted as C<sub>3</sub>N<sub>4</sub>-rGO-*x*, where *x* represents the mass ratio of melamine to rGO during the synthesis process. For example, the composite C<sub>3</sub>N<sub>4</sub>-rGO-150 was prepared by calcining the mixture of 20 mg of rGO and 3000 mg of melamine at 500 °C  
35 for 3 h with a 5 °C/min increasing rate. Pure C<sub>3</sub>N<sub>4</sub> was also obtained by calcining melamine at 500 °C for 3 h.

*Synthesis of C<sub>3</sub>N<sub>4</sub>-rGO-WO<sub>3</sub> and C<sub>3</sub>N<sub>4</sub>-WO<sub>3</sub> composites*: The ternary composites are noted as C<sub>3</sub>N<sub>4</sub>-rGO-*x*-WO<sub>3</sub> *m-n*, *m* representing the initial reacting mass of C<sub>3</sub>N<sub>4</sub>-rGO-*x* in mg, *n*  
40 representing that of Na<sub>2</sub>WO<sub>4</sub>·2H<sub>2</sub>O. Taking C<sub>3</sub>N<sub>4</sub>-rGO-150-WO<sub>3</sub> 400-260 for example, 400 mg of C<sub>3</sub>N<sub>4</sub>-rGO-150 and 260 mg of Na<sub>2</sub>WO<sub>4</sub>·2H<sub>2</sub>O (99%, Aldrich) were mixed in 30 mL of deionized water and kept stirring at ca. 300 rpm for 12 h. Then the pH value was adjusted to 2 using diluted HCl solution. After  
45 further stirring at ca. 300 rpm for another 12 h, the suspension was transferred into a Teflon-lined steel autoclave and kept at 160 °C for 18 h. The C<sub>3</sub>N<sub>4</sub>-WO<sub>3</sub> composite was obtained by the same method except for using pure C<sub>3</sub>N<sub>4</sub> instead of C<sub>3</sub>N<sub>4</sub>-rGO composites. After hydrothermal reaction, the resulted composites  
50 were separated by centrifugation at 4000 rpm and washed with distilled water for several times before dried at 90 °C for 3 h.

*Pt-loading on the C<sub>3</sub>N<sub>4</sub>-rGO, C<sub>3</sub>N<sub>4</sub>-rGO-WO<sub>3</sub> and C<sub>3</sub>N<sub>4</sub>-WO<sub>3</sub> composites*: Pt was firstly loaded onto the specimen by impregnation method: proper amount of H<sub>2</sub>PtCl<sub>6</sub> solution (ca. 4  
55 mL) was impregnated into the sample powders by evaporating the solvent of the mixed suspension at 90 °C until dry. For H<sub>2</sub>-evolution test by C<sub>3</sub>N<sub>4</sub>-rGO composites, these Pt-loaded samples

were used in the presence of triethanolamine (TEOA) as sacrificial agent. For overall water splitting test by C<sub>3</sub>N<sub>4</sub>-rGO-  
60 WO<sub>3</sub> and C<sub>3</sub>N<sub>4</sub>-WO<sub>3</sub> composites, these Pt-loaded samples were further reduced by NaBH<sub>4</sub> solution in Ar protection. For example, 200 mg of C<sub>3</sub>N<sub>4</sub>-rGO-150-WO<sub>3</sub> 400-260 loaded with 1 wt% Pt was dissolved in 30 mL of deionized water and purged with Ar for 30 min before adding 5 mg of NaBH<sub>4</sub>. After 2 h for reduction,  
65 the suspension was centrifugated and washed with distilled water for several times. The resulted slurry was then used for photocatalytic test.

*Material Characterizations*: Specimens were characterized by XRD on a PANalytical Empyrean Reflection diffractometer with  
70 a Cu K $\alpha$  source ( $\lambda = 1.541$  Å). TEM analysis was performed on a JEM-2011. XPS were tested by an ESCALAB 250 and all binding energies were referenced to the C 1s peak at 284.6 eV. A UV-Vis spectrophotometer (JASCO-V550) was used for testing the optical absorbance spectra.

75 *Photocatalytic measurement*: The measurement was performed with a home-made Teflon reactor with top window sealed by a pyrex glass. In H<sub>2</sub>-evolution test by C<sub>3</sub>N<sub>4</sub>-rGO composites loaded with 1 wt% Pt, 200 mg of photocatalyst was dispersed into 100 mL of water and 10 mL of TEOA was added as sacrificial agent.  
80 In O<sub>2</sub>-evolution test by WO<sub>3</sub>·1/3H<sub>2</sub>O, 100 mg of WO<sub>3</sub>·1/3H<sub>2</sub>O powder was dispersed into 100 mL of water with 10 mmol/L of AgNO<sub>3</sub> as an electron acceptor. The reactor was firstly purged with pure Ar to remove air from the reaction system, then the solution was irradiated by a 250 W iron doped metal halide UV-  
85 Vis lamp (UV Light Technology Limited, UK) with a UV cut-off filter ( $\lambda > 420$  nm) and the amount of H<sub>2</sub> or O<sub>2</sub> produced was determined by gas chromatography (Agilent 3000 Micro Gas Chromatograph with a TCD detector, using argon carrier gas). The H<sub>2</sub>- and O<sub>2</sub>-evolution half reaction results shown in  
90 supporting information demonstrated their activity under visible light. The mediator-free Z-scheme overall water splitting reaction trials were performed in the same top-irradiation system. During these trials, 200 mg of Pt-loaded C<sub>3</sub>N<sub>4</sub>-rGO-WO<sub>3</sub> or C<sub>3</sub>N<sub>4</sub>-WO<sub>3</sub> composites were suspended in 100 mL of deionized water, but no  
95 TEOA was added. The evolved gas composition in the sealed reactor was measured by gas chromatography.

*Quantum yield efficiency measurement*: The apparent quantum yield (AQY) of the Z-scheme water splitting with a two-photon excitation process was measured using the same reactor with the  
100 addition of a band-pass filter (420 nm,  $\Delta\lambda_{1/2} = 10$  nm). The AQY values were calculated using the following equation:<sup>22</sup>

$$\text{AQY} (\%) = [4 \times n(\text{H}_2)] / n(\text{photons}) \times 100 \quad (1)$$

where  $n(\text{H}_2)$  and  $n(\text{photons})$  represent the quantities of evolved H<sub>2</sub> molecules and the number of incident photons, respectively.

105 The total number incident photons were determined using a grating spectroradiometer (Apogee Instruments, Inc, Model MQ-200) and the the incident photon power in the apparent quantum yield measurement is about 120  $\mu\text{mol m}^{-2} \text{s}^{-1}$ .

## 3. Results and Discussion

110 Figure 1 shows the typical XRD patterns of WO<sub>3</sub> and C<sub>3</sub>N<sub>4</sub>-rGO-150-WO<sub>3</sub> composites resulting from the hydrothermal reaction of Na<sub>2</sub>WO<sub>4</sub>·2H<sub>2</sub>O without or with different contents of C<sub>3</sub>N<sub>4</sub>-rGO-150. The XRD pattern in Figure 1a denotes the presence of orthorhombic tungsten oxide one third hydrate (WO<sub>3</sub>·1/3H<sub>2</sub>O,

JCPDS Card no. 54-1012), and the characteristic peak from  $C_3N_4$  located at around 27 degree increased with the increment of  $C_3N_4$ -rGO-150 content, as shown in Figure 1b and 1c. There are no obvious diffraction peaks for  $WO_3 \cdot 1/3H_2O$  in Figure 1c, which may be due to the large molar ratio of  $C_3N_4$  to  $WO_3$  in  $C_3N_4$ -rGO-150- $WO_3$  1000-260 (ca. 13.8 calculated from the added amount). If considering the smaller density and bigger particle size of  $C_3N_4$  than  $WO_3$  nanoparticles in  $C_3N_4$ -rGO-150- $WO_3$  1000-260, the XRD diffraction density of  $C_3N_4$  is much stronger than that of  $WO_3$  nanoparticles. Therefore, the diffraction peaks of  $WO_3 \cdot 1/3H_2O$  were properly overlapped by that of  $C_3N_4$ . In addition, the crystallinity of  $WO_3$  may be also poor because of the dispersion of  $C_3N_4$  particles.

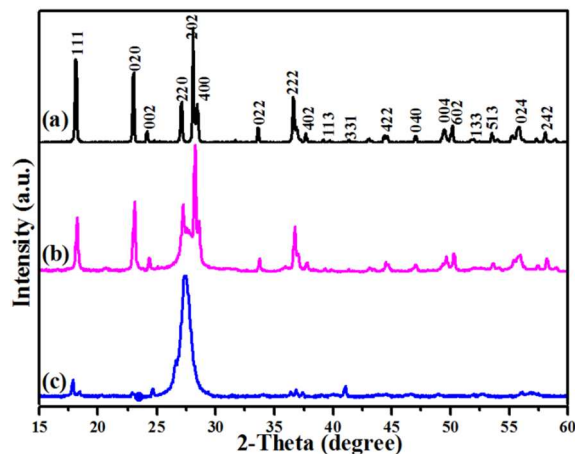


Figure 1. XRD patterns of pure  $WO_3$  (a),  $C_3N_4$ -rGO-150- $WO_3$  400-260 (b) and  $C_3N_4$ -rGO-150- $WO_3$  1000-260 (c).

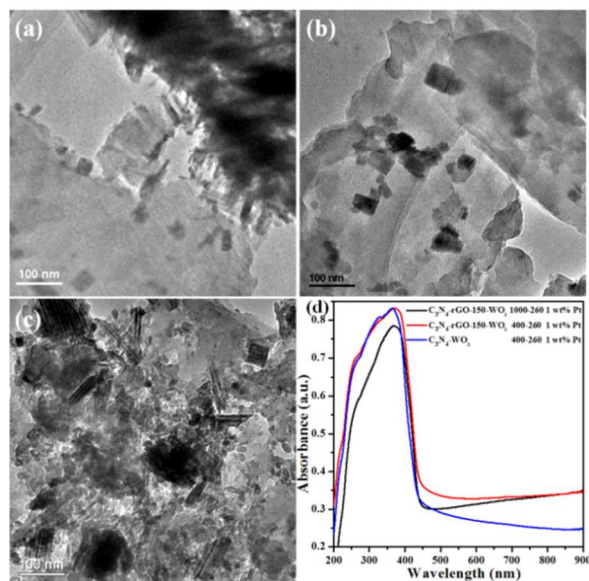


Figure 2. TEM images of  $C_3N_4$ -rGO-150- $WO_3$  400-260 (a),  $C_3N_4$ -rGO-150- $WO_3$  1000-260 (b),  $C_3N_4$ -rGO-150- $WO_3$  400-260 loaded with 1 wt% Pt after photocatalytic test (c); The UV-Vis light absorbance spectra (converted from the corresponding reflectance spectra) of three typical samples loaded with 1 wt% Pt (d).

Figure 2a and 2b show the TEM images of  $C_3N_4$ -rGO-150- $WO_3$  400-260 and  $C_3N_4$ -rGO-150- $WO_3$  1000-260, respectively. It is obvious that in the hydrothermal reaction, the higher  $Na_2WO_4 \cdot 2H_2O/C_3N_4$ -rGO-150 ratio means that the more  $WO_3$

particles are not loaded on the surface of  $C_3N_4$ -rGO-150 but must be independent of it, while in  $C_3N_4$ -rGO-150 1000-260, almost no independent  $WO_3$  particles exist. By loading Pt as co-catalyst, efficient  $H_2$ -evolution performance can be realized. Figure 2c and Figure S1 (see in Supporting Information) show the TEM images of  $C_3N_4$ -rGO-150 400-260 loaded with 1 wt% Pt after several periods of photocatalytic water splitting tests, indicating that Pt is mainly distributed onto the surface of  $C_3N_4$  maybe due to its stronger chelating ability to  $Pt^{2+}$ . The typical UV-Vis light absorbance spectra in Figure 2d also indicate that there were no obvious differences in the absorbance between the composites with different  $WO_3$  contents, while adding rGO indeed increased the absorption toward the visible light.

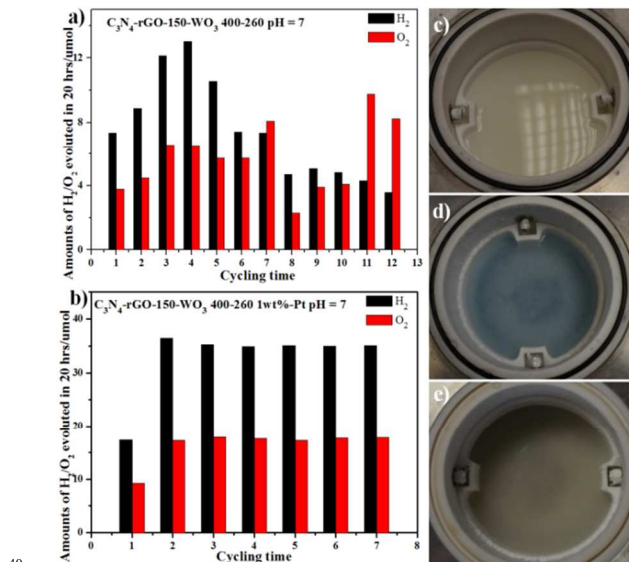


Figure 3. The performance of the cycling test for  $C_3N_4$ -rGO-150- $WO_3$  400-260 without (a) and with (b) Pt under pH = 7; the  $C_3N_4$ -rGO-150- $WO_3$  400-260 without Pt before photo-reaction (c) and after six cycle of photo-reaction (d); the sample  $C_3N_4$ -rGO-150- $WO_3$  400-260 with Pt after six cycles of photo-reaction (e).

We used the as-prepared  $C_3N_4$ -rGO-150- $WO_3$  400-260 without loading Pt as photocatalyst for cycling water-splitting test under visible light (Figure 3). As shown in Figure 3a, in the initial four cycles, the performance increased but then decayed on further cycling. The best performance is only about 12  $\mu mol H_2$  in 20 hours' irradiation. After loading Pt as co-catalyst, the case is much different, as shown in Figure 3b. The  $H_2$ -evolution performance is very stable from the second cycle and the final amount of  $H_2$  produced in 20 hours is as high as 35  $\mu mol$  and the produced  $O_2$  is about half in  $\mu mol$  compared with that of  $H_2$ . It is also noted that without loaded Pt, the photocatalyst underwent obvious color change during the photo-reaction as shown in Figure 3c and 3d, where the milk-white suspension changed into blue after six cycles of test. According to much reported research on the photochromogenic  $WO_3$ , when irradiated at a photo energy higher than its band gap (2.8 eV), photochromism would occur, in which the photo-generated electron-hole would lead to the reduction of  $W^{6+}$  into blue-colored  $W^{5+}$ .<sup>23-28</sup> While after loaded with Pt nanoparticles, the photocatalyst became just a little darker comparing with that of the milk-white  $C_3N_4$ -rGO-150- $WO_3$  400-260, and no color changed during the photo-reaction, as shown in

**Table 1.** Overall water splitting under visible light by C<sub>3</sub>N<sub>4</sub>-WO<sub>3</sub> system in the presence and absence of rGO<sup>a</sup>

No.	Hydrothermal conditions				Activity after 20 h irradiation		
	Type of C <sub>3</sub> N <sub>4</sub> or C <sub>3</sub> N <sub>4</sub> -rGO	C <sub>3</sub> N <sub>4</sub> or C <sub>3</sub> N <sub>4</sub> -rGO (mg)	Na <sub>2</sub> WO <sub>4</sub> ·2H <sub>2</sub> O (mg)	Amount of loaded Pt <sup>b</sup>	pH <sup>c</sup>	H <sub>2</sub> (μmol)	O <sub>2</sub> (μmol)
1	Pure C <sub>3</sub> N <sub>4</sub>	400	0	1 wt% Pt	7	trace	Trace
2	C <sub>3</sub> N <sub>4</sub> -rGO-150	400	0	1 wt% Pt	7	3.3	1.1
3	C <sub>3</sub> N <sub>4</sub> -rGO-150	400	260	1 wt% Pt	7	35.1	18.5
4	C <sub>3</sub> N <sub>4</sub> -rGO-80	400	260	1 wt% Pt	7	26.1	14.1
5	C <sub>3</sub> N <sub>4</sub> -rGO-50	400	260	1 wt% Pt	7	20.8	11.2
6	Pure C <sub>3</sub> N <sub>4</sub>	400	260	1 wt% Pt	7	30.3	14.8
7	Pure C <sub>3</sub> N <sub>4</sub>	1000	260	1 wt% Pt	7	29.9	14.5
8	C <sub>3</sub> N <sub>4</sub> -rGO-150	1000	260	1 wt% Pt	7	48.1	24.5
9	C <sub>3</sub> N <sub>4</sub> -rGO-50	400	260	3 wt% Pt	7	6.0	3.3
10	C <sub>3</sub> N <sub>4</sub> -rGO-150	400	260	3 wt% Pt	7	11.0	5.0
11	C <sub>3</sub> N <sub>4</sub> -rGO-150	1000	260	1 wt% Pt	3	11.4	30.5
12	C <sub>3</sub> N <sub>4</sub> -rGO-150	1000	260	1 wt% Pt	5	29.0	15.1
13	C <sub>3</sub> N <sub>4</sub> -rGO-150	1000	260	1 wt% Pt	8	53.5	26.8
14	C <sub>3</sub> N <sub>4</sub> -rGO-150	1000	260	1 wt% Pt	10	56.6	29.2

<sup>a</sup>) Conditions: photocatalyst (200 mg in total) in water (100 mL); light source, 250 W iron-doped metal halide ultraviolet-visible lamp, with a cut-off filter ( $\lambda > 420$  nm); top-irradiation cell with a quartz glass. <sup>b</sup>) Pt was loaded by first impregnation of H<sub>2</sub>PtCl<sub>6</sub>, the lateral reduction with NaBH<sub>4</sub> solution and the last washing for several times before using as photocatalyst in muddy; <sup>c</sup>) The pH of the suspension in the photocatalytic test system.

Figure 3e. It is now discovered that the loaded Pt is able to inhibit the color changing, which may be due to the efficient electron capture by the loaded Pt nanoparticles. The gas generation amount dependence on reaction time shown in Figure S2 for C<sub>3</sub>N<sub>4</sub>-rGO-150-WO<sub>3</sub> 400-260 loaded with 1 wt% Pt indicates that gaseous products evolve linearly for the next 12 h with a ratio of ca. 2:1 (H<sub>2</sub> and O<sub>2</sub> : 1.52 and 0.74 μmol h<sup>-1</sup>) under visible light.

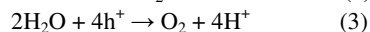
To investigate the effects of graphene content, the mass ratio of C<sub>3</sub>N<sub>4</sub> (or C<sub>3</sub>N<sub>4</sub>/rGO) and WO<sub>3</sub>, the pH in the photocatalytic system and the amount of loaded Pt on the water-splitting performance, we tested the H<sub>2</sub>/O<sub>2</sub> evolution amount with different photocatalysts and in different conditions. As indicated by No. 1 and 2 in Table 1, when using only C<sub>3</sub>N<sub>4</sub> loaded with 1 wt% Pt in the nonsacrificial condition, no water splitting occurred, while when using C<sub>3</sub>N<sub>4</sub>-rGO-150 composite loaded with 1 wt% Pt, the produced H<sub>2</sub> is about 3.3 μmol in 20 hours' irradiation. In Jorge et al's work, C<sub>3</sub>N<sub>4</sub> was used for H<sub>2</sub> and O<sub>2</sub> evolution from water half-splitting with methanol and Ag<sup>+</sup> as sacrificial agent, respectively.<sup>29</sup> In our photocatalytic reaction test, No. 2, the little water splitting activity should come out from the reduction and oxidation of water due to the improved electro-hole separation by graphene. In No. 3-6, it is also shown that different rGO contents in the C<sub>3</sub>N<sub>4</sub>-rGO composites have great effect on the water-splitting activity. Both no rGO or too much rGO in the C<sub>3</sub>N<sub>4</sub>-rGO composites gives worse performance for the H<sub>2</sub>/O<sub>2</sub> evolution than that of the C<sub>3</sub>N<sub>4</sub>-rGO-150 composite (No. 3), even though the C<sub>3</sub>N<sub>4</sub>-rGO-150 composite only displays an enhancement of 15.8% for the H<sub>2</sub>/O<sub>2</sub> evolution over pure C<sub>3</sub>N<sub>4</sub> and WO<sub>3</sub> system (No. 6). We have also investigated the rGO effect by testing the H<sub>2</sub>-evolution performance using different C<sub>3</sub>N<sub>4</sub>-rGO composites using TEOA as sacrificial agent and Pt as co-catalyst (see more details in Figure S3 and Table S1 in Supporting Information). It is implied that rGO has two synergetic effects, one is to prevent the hole-electron recombination by transferring electrons, the other is to prevent the efficient irradiation due to its opacity and light

scattering.<sup>30-32</sup> An appropriate amount of graphene in the C<sub>3</sub>N<sub>4</sub>-rGO composite would improve the electron transfer and further prevent the charge carrier-recombination,<sup>33-35</sup> thus a little enhancement occurred for C<sub>3</sub>N<sub>4</sub>-rGO-150 composite with Pt as co-catalyst.

The results for No. 3 and 8 in Table 1 show that sample C<sub>3</sub>N<sub>4</sub>-rGO-150-WO<sub>3</sub> 1000-260 displays a higher performance by 37% than that of C<sub>3</sub>N<sub>4</sub>-rGO-150-WO<sub>3</sub> 400-260 under the same condition (i.e., loaded with 1 wt% Pt in pH = 7), indicating too much WO<sub>3</sub> deposited on the surface of C<sub>3</sub>N<sub>4</sub>-rGO-150 will prevent the incident light reaching to the C<sub>3</sub>N<sub>4</sub>-rGO-150 surface, which results in the weakened photoexcitation of C<sub>3</sub>N<sub>4</sub>-rGO-150.<sup>36</sup> However, for pure C<sub>3</sub>N<sub>4</sub> and WO<sub>3</sub> system, there is no obvious change in the water-splitting performance with different mass ratios of C<sub>3</sub>N<sub>4</sub> to WO<sub>3</sub> (No. 6 and 7 in Table 1). These results show that WO<sub>3</sub> amount has more obvious influence in C<sub>3</sub>N<sub>4</sub>-rGO-150 system than pure C<sub>3</sub>N<sub>4</sub> system, further suggesting that rGO is able to play a significant role in the Z-scheme water-splitting system because of its good conductivity and its function as promising electron mediator for transferring the photo-generated electrons from WO<sub>3</sub> to the photo-generated holes in C<sub>3</sub>N<sub>4</sub>. The effect of loaded Pt amount is also revealed from comparison between No. 5 and 9 or No. 3 and 10. Too much Pt has negative effect for the gas evolution, as proved by other reports.<sup>37-39</sup>

According to previous research on Z-scheme photocatalyst system, to ensure the charge transfer, intimate physical interaction between the two photocatalysts was often realized by the aggregation of the two photocatalysts under some appropriate pH.<sup>8,11</sup> In our case, the effect of pH on the water-splitting activity was also investigated using C<sub>3</sub>N<sub>4</sub>-rGO-150-WO<sub>3</sub> 1000-260 as target. It is found that with the increasing of pH, the gas evolution rate is gradually increased (No. 8, 11-14). When the pH equals to 3, the produced H<sub>2</sub> is as low as 11.4 μmol in 20 hours. Since WO<sub>3</sub> is inherently instable at high pH, we did not test the performance

under higher pH conditions. Thus the pH effect should not come from the aggregation level but from the kinetic rate of the H<sub>2</sub> and O<sub>2</sub> evolution reactions, which can be expressed as followings:



It can be inferred that although pH has the conflicting effect for Equation 2 and 3, a higher pH is beneficial to the whole performance. This is despite that under acidic condition, H<sub>2</sub>-evolution reaction is relatively favorable, the associated negative effect for the O<sub>2</sub> evolution would trade off the little benefit since the water oxidation depends on the adsorbed OH<sup>-</sup> ions onto the WO<sub>3</sub> surface and their following oxidation by multiple photo-generated holes.<sup>40</sup> Thus under more alkaline conditions, the final H<sub>2</sub>/O<sub>2</sub>-evolution performance turns out higher, and these results indicate that the O<sub>2</sub>-evolution reaction is the rate-determining process.

We also prepared a C<sub>3</sub>N<sub>4</sub>-WO<sub>3</sub> composite via two other methods, one by calcining WO<sub>3</sub> nanoparticles and C<sub>3</sub>N<sub>4</sub> mixture at 350 °C and the other by hydrothermal treatment of WO<sub>3</sub> nanoparticles and C<sub>3</sub>N<sub>4</sub> mixture at 160 °C. Both of the as-prepared mixture were loaded with 1 wt% Pt before photocatalytic test. And for the two cases, no H<sub>2</sub> was detected. It is confirmed that the hydrothermal condition results in the intimate contact between C<sub>3</sub>N<sub>4</sub> (or C<sub>3</sub>N<sub>4</sub>-rGO) and WO<sub>3</sub> due to the special high-temperature and high-pressure environment. And the *in-situ* formation of WO<sub>3</sub> particles on C<sub>3</sub>N<sub>4</sub> framework also contributes the intimate interaction between the two photocatalysts.

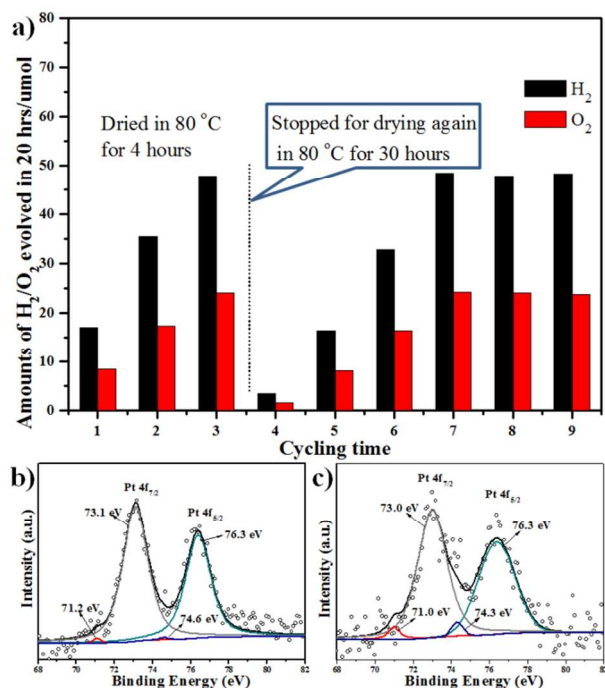


Figure 4. The cycling performance of the sample (C<sub>3</sub>N<sub>4</sub>-rGO-150-WO<sub>3</sub> 1000-260 loaded with 1 wt% Pt) dried after several photo-test cycles as fresh slurry (a); XPS of the sample dried in air for 30 hours (b); XPS of the fresh wet sample dried in Ar (c).

It is worth to note that the photocatalysts used in Table 1 were fresh wet samples from the reduction by NaBH<sub>4</sub> without drying. And we also tried to dry the sample C<sub>3</sub>N<sub>4</sub>-rGO-150-WO<sub>3</sub> 1000-

260 (loaded with 1 wt% Pt) after several cycling tests with stable performance. Interestingly, after dried in air at 80 °C for 4 hours, the sample showed a lower activity compared with its stable performance before drying, and only after 3 cycles, the performance was recovered, as shown in Figure 4. Then the sample was dried again at 80 °C for 30 hours, after which the H<sub>2</sub>/O<sub>2</sub> evolution became even worse and also recovered after 4 cycles (Figure 4a). We investigated the XPS of the sample dried in air at 80 °C for 30 hours and the fresh wet sample dried in Ar. The XPS survey spectrum shown in Figure S4 (see in Supporting Information) demonstrated the existence of C, N, O, Pt and W, but no Na was observed. Although both of the samples showed a high content of PtO<sub>x</sub> (indicated by the Pt 4f<sub>7/2</sub> and Pt 4f<sub>5/2</sub> peaks centered at ca. 73.0 eV and 76.3 eV, respectively),<sup>41</sup> the metallic Pt content in the sample dried in Ar is obviously higher than that dried in air (indicated by the Pt 4f<sub>7/2</sub> and Pt 4f<sub>5/2</sub> peaks centered at ca. 71.0 eV and 74.3 eV, respectively), as shown in Figure 4b and 4c.<sup>42</sup> Therefore, it is inferred that the evolved H<sub>2</sub> would reduce PtO<sub>x</sub> into Pt metal during the irradiation and the activity of the sample is quite sensitive to the Pt metal content.

The evolution of H<sub>2</sub> from water splitting was further confirmed by using D<sub>2</sub>O as the solvent in the suspension of photocatalyst. The evolved gas mixture was then detected by the mass spectra and the results were shown in Figure S5 (see in Supporting Information). The extra signal located at 4 amu is due to evolved D<sub>2</sub>, which is absent in that of the background gas. We also measured the apparent quantum yield efficiency under monochromatic light at 420 nm. The sample C<sub>3</sub>N<sub>4</sub>-rGO-150-WO<sub>3</sub> 1000-260 (loaded with 1 wt% Pt) under neutral condition shows an AQY efficiency of ca. 0.9% while the homologous sample without rGO shows a smaller value (i.e., 0.7%), further demonstrating the positive effect of rGO.

Although Martin et al.,<sup>10</sup> recently reported a similar Z-scheme water splitting on the base of C<sub>3</sub>N<sub>4</sub> and WO<sub>3</sub> (or BiVO<sub>4</sub>), their performance is strongly dependent on the redox mediator type (i.e., I/I<sub>3</sub><sup>-</sup>) and the pH. However, in our C<sub>3</sub>N<sub>4</sub>-rGO (or C<sub>3</sub>N<sub>4</sub>) and WO<sub>3</sub> composite system, no redox mediator is needed for the water-splitting photocatalytic test, which further infers that the intimate contact resulted from hydrothermal condition is of benefit to the H<sub>2</sub>/O<sub>2</sub> evolution in the two-photo excited Z-scheme system. Figure 5 shows a tentatively proposed mechanism for the H<sub>2</sub>/O<sub>2</sub> evolution by the C<sub>3</sub>N<sub>4</sub>-WO<sub>3</sub> composite with or without the mediating of rGO. According to previous study, the CB and VB positions of WO<sub>3</sub> are located about +0.41 eV and +3.18 eV,<sup>43</sup> while those of C<sub>3</sub>N<sub>4</sub> are about -1.13 eV and +1.57 eV.<sup>19</sup> It is not difficult to infer that under irradiation, O<sub>2</sub> could be evolved from WO<sub>3</sub> surface and H<sub>2</sub> from C<sub>3</sub>N<sub>4</sub> surface. Considering the Pt function as discussed above, H<sub>2</sub> is more readily evolved from the surface of Pt than that of C<sub>3</sub>N<sub>4</sub>. Therefore, water is oxidized by the photo-induced holes in the VB of WO<sub>3</sub> and reduced by the electrons on Pt trapped from the CB of C<sub>3</sub>N<sub>4</sub>. The electrons on CB of WO<sub>3</sub> are able to combine with the holes in VB of C<sub>3</sub>N<sub>4</sub> at the interface due to the intimate contact. rGO successfully functions as a positive electron mediator because of its good conductivity for electron migration, its sturdy contact with C<sub>3</sub>N<sub>4</sub> resulted from its calcination with the precursor (i.e., melamine), and its good contact with WO<sub>3</sub> particles under the hydrothermal conditions.

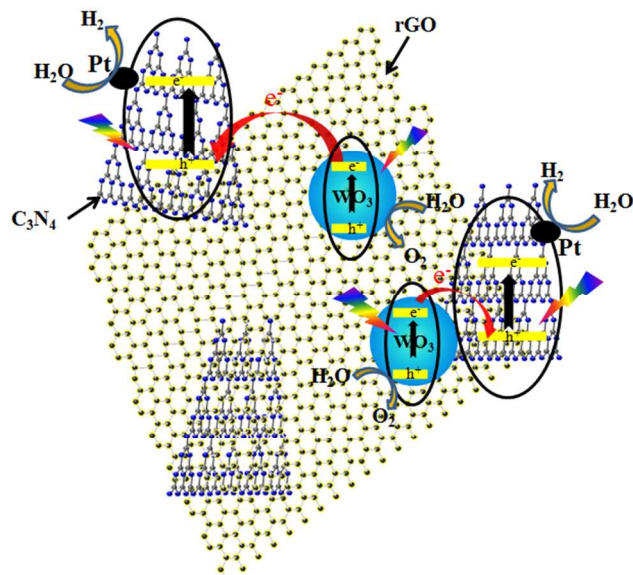


Figure 5. Proposed mechanism for the  $\text{H}_2/\text{O}_2$  evolution by  $\text{C}_3\text{N}_4$ - $\text{WO}_3$  composite with or without the mediating of rGO.

#### 4. Conclusions

In summary, we have introduced a mediator-free Z-scheme system design based on  $\text{C}_3\text{N}_4$  by utilizing  $\text{WO}_3$  as  $\text{O}_2$  photocatalyst for the first time, where  $\text{C}_3\text{N}_4$  and  $\text{WO}_3$  are combined as composites through a facile hydrothermal method. Successful water splitting under visible light ( $\lambda > 420$  nm) can be realized without any redox mediator when Pt is loaded on the surface of the composites. More importantly, rGO is introduced into these composites to form  $\text{C}_3\text{N}_4$ -rGO- $\text{WO}_3$  composites and this shows positive effect on the performance in an optimized amount. The highest  $\text{H}_2/\text{O}_2$  evolution rate is about 2.84 and 1.46  $\mu\text{mol h}^{-1}$  under visible light ( $\lambda > 420$  nm) with the quantum yield of 0.9% at 420 nm. Although the resulted performance is not in the highest level for water splitting, the newly proposed methodology for constructing heterostructure through hydrothermal method will pave a way for more efficient overall water splitting with two-photo excited Z-scheme system in the absence of redox mediator.

#### Acknowledgements

The authors gratefully thank the Engineering and Physical Sciences Research Council (EPSRC) platform grant EP/K006800/1, EP/K036769/1 and EP/K022237/1 for financial support.

#### Notes and references

School of Chemistry, University of St Andrews, St Andrews, Fife, UK: Fax: +44 (0)1334463808; Tel: +44(0)1334463817; E-mail: jst@st-andrews.ac.uk.

† Electronic Supplementary Information (ESI) available: [ $\text{H}_2$  evolution performance by  $\text{C}_3\text{N}_4$ -rGO composites with TEOA as sacrificial agent under visible light, rGO contents in different  $\text{C}_3\text{N}_4$ -rGO composites, and the mass spectra results using  $\text{D}_2\text{O}$ ]. See DOI: 10.1039/b000000x/

‡ These authors contributed equally to this work.

1. N. S. Lewis, *Science*, 2007, **315**, 798-801.

2. R. Abe, T. Takata, H. Sugihara and K. Domen, *Chem. Commun.*, 2005, 3829-3831.
3. M. Tabata, K. Maeda, M. Higashi, D. Lu, T. Takata, R. Abe and K. Domen, *Langmuir*, 2010, **26**, 9161-9165.
4. H. Kato, M. Hori, R. Kouta, Y. Shimodaira and A. Kudo, *Chem. Lett.*, 2004, **33**, 1348-1349.
5. R. M. Navarro, M. C. Alvarez-Galvan, J. A. Villoria de la Mano, S. M. Al-Zahrani and J. L. G. Fierro, *Energy Environ. Sci.*, 2010, **3**, 1865-1882.
6. S. J. A. Moniz, S. A. Shevlin, D. J. Martin, Z.-X. Guo and J. Tang, *Energy Environ. Sci.*, 2015, **8**, 731-759.
7. Y. Miseki, S. Fujiiyoshi, T. Gunji and K. Sayama, *Catal. Sci. Technol.*, 2013, **3**, 1750-1756.
8. Y. Sasaki, H. Nemoto, K. Saito and A. Kudo, *J. Phys. Chem. C*, 2009, **113**, 17536-17542.
9. M. Higashi, R. Abe, K. Teramura, T. Takata, B. Ohtani and K. Domen, *Chem. Phys. Lett.*, 2008, **452**, 120-123.
10. D. J. Martin, P. J. T. Reardon, S. J. A. Moniz and J. Tang, *J. Am. Chem. Soc.*, 2014, **136**, 12568-12571.
11. A. Iwase, Y. H. Ng, Y. Ishiguro, A. Kudo and R. Amal, *J. Am. Chem. Soc.*, 2011, **133**, 11054-11057.
12. K. Yamaguti and S. Sato, *J. Chem. Soc. Faraday Trans. 1: Phys. Chem. Condensed Phases*, 1985, **81**, 1237-1246.
13. K. Maeda, K. Teramura, D. Lu, N. Saito, Y. Inoue and K. Domen, *Angew. Chem. Int. Edit.*, 2006, **45**, 7806-7809.
14. F. Goettmann, A. Fischer, M. Antonietti and A. Thomas, *Angew. Chem. Int. Edit.*, 2006, **45**, 4467-4471.
15. F. Goettmann, A. Fischer, M. Antonietti and A. Thomas, *Chem. Commun.*, 2006, 4530-4532.
16. X. Wang, K. Maeda, A. Thomas, K. Takanabe, G. Xin, J. M. Carlsson, K. Domen and M. Antonietti, *Nat. Mater.*, 2009, **8**, 76-80.
17. X. Wang, K. Maeda, X. Chen, K. Takanabe, K. Domen, Y. Hou, X. Fu and M. Antonietti, *J. Am. Chem. Soc.*, 2009, **131**, 1680-1681.
18. Z. Zhao, Y. Sun and F. Dong, *Nanoscale*, 2015, **7**, 15-37.
19. S. C. Yan, S. B. Lv, Z. S. Li and Z. G. Zou, *Dalton Trans.*, 2010, **39**, 1488-1491.
20. H. Kominami, K.-i. Yabutani, T. Yamamoto, Y. Kera and B. Ohtani, *J. Mater. Chem.*, 2001, **11**, 3222-3227.
21. G. Zhao, J. Li, X. Ren, C. Chen and X. Wang, *Environ. Sci. Technol.*, 2011, **45**, 10454-10462.
22. Q. Wang, T. Hisatomi, S. S. K. Ma, Y. Li and K. Domen, *Chem. Mater.*, 2014, **26**, 4144-4150.
23. C. Bechinger, G. Oefinger, S. Herminghaus and P. Leiderer, *J. Appl. Phys.*, 1993, **74**, 4527-4533.
24. J. G. Zhang, D. K. Benson, C. E. Tracy, S. K. Deb, A. W. Czanderna and C. Bechinger, *J. Electrochem. Soc.*, 1997, **144**, 2022-2026.
25. Y. He, Z. Wu, L. Fu, C. Li, Y. Miao, L. Cao, H. Fan and B. Zou, *Chem. Mater.*, 2003, **15**, 4039-4045.
26. W. Morales, M. Cason, O. Aina, N. R. de Tacconi and K. Rajeshwar, *J. Am. Chem. Soc.*, 2008, **130**, 6318-6319.
27. G. Hodes, D. Cahen and J. Manassen, *Nature*, 1976, **260**, 312-313.
28. M. A. Butler, R. D. Nasby and R. K. Quinn, *Solid State Commun.*, 1976, **19**, 1011-1014.
29. A. B. Jorge, D. J. Martin, M. T. S. Dhanoa, A. S. Rahman, N. Makwana, J. Tang, A. Sella, F. Corà, S. Firth, J. A. Darr and P. F. McMillan, *J. Phys. Chem. C*, 2013, **117**, 7178-7185.
30. W. Ho, J. C. Yu, J. Lin, J. Yu and P. Li, *Langmuir*, 2004, **20**, 5865-5869.
31. J. Yu, Y. Hai and M. Jaroniec, *J. Colloid Interf. Sci.*, 2011, **357**, 223-228.
32. J. Yu, X. Zhao and Q. Zhao, *Thin Solid Films*, 2000, **379**, 7-14.
33. X.-H. Li, J.-S. Chen, X. Wang, J. Sun and M. Antonietti, *J. Am. Chem. Soc.*, 2011, **133**, 8074-8077.
34. Q. Xiang, J. Yu and M. Jaroniec, *J. Phys. Chem. C*, 2011, **115**, 7355-7363.
35. Y. Li, H. Zhang, P. Liu, D. Wang, Y. Li and H. Zhao, *Small*, 2013, **9**, 3336-3344.
36. P. Zhou, J. Yu and M. Jaroniec, *Adv. Mater.*, 2014, **26**, 4920-4935.
37. M. Hara, J. Nunoshige, T. Takata, J. N. Kondo and K. Domen, *Chem. Commun.*, 2003, 3000-3001.

- 
38. N. Bao, L. Shen, T. Takata and K. Domen, *Chem. Mater.*, 2007, **20**, 110-117.
39. K. Maeda, X. Wang, Y. Nishihara, D. Lu, M. Antonietti and K. Domen, *J. Phys. Chem. C*, 2009, **113**, 4940-4947.
- 5 40. Y. Zhong, K. Ueno, Y. Mori, X. Shi, T. Oshikiri, K. Murakoshi, H. Inoue and H. Misawa, *Angew. Chem.*, 2014, **126**, 10518-10522.
41. G. M. Bancroft, I. Adams, L. L. Coatsworth, C. D. Bennewitz, J. D. Brown and W. D. Westwood, *Anal. Chem.*, 1975, **47**, 586-588.
42. G. Johansson, J. Hedman, A. Berndtsson, M. Klasson and R. Nilsson, *J. Electron Spectrosc. Relat. Phenom.*, 1973, **2**, 295-317.
- 10 43. S. J. Hong, S. Lee, J. S. Jang and J. S. Lee, *Energy Environ. Sci.*, 2011, **4**, 1781-1787.

15

A mediator-free Z-scheme overall water splitting photocatalyst system is achieved through the use of  $C_3N_4$  ( $H_2$  generation catalyst) and  $WO_3$  ( $O_2$  generation catalyst) composite from a hydrothermal method, and Pt as co-catalyst under visible light ( $\lambda > 420$  nm).

